Journal of Physical and Theoretical Chemistry
of Islamic Azad University of Iran, 18 (4) 1-18: Winter 2022
(J. Phys. Theor. Chem. IAU Iran)
ISSN 1735-2126

Removal Studies of Methyl Orange Dye Using *Asparagus plant*-capped Fe_3O_4NPs from Aqueous Solutions

Alireza Geramizadegan *

Department of Chemistry, Dashtestan Branch, Islamic Azad University, Dashtestan, Iran

Received November 2022; Accepted November 2022

ABSTRACT

The applicability of *Asparagus plant* functionalized with iron oxide nanoparticles synthesis for eliminating dyes from aqueous media has been confirmed. The techniques including FT-IR, BET, XRD and SEM for investigation showed the applicability of Asparagus plant functionalized with iron oxide nanoparticles as adsorbent for proper deletion of Methyl Orange dye from aqueous, and article the values of 15 mgL^{-1}, 0.1 g, 7.0, 20.0 min were considered as the ideal values for Methyl Orange dye concentration, adsorbent mass, pH value and contact time respectively. The adsorption equilibrium and kinetic data were fitted with the Langmuir monolayer isotherm model (q: 0.9915) and pseudo-second order kinetics (R^2: 0.998) with maximum adsorption capacity (qmax: 167.7 mgg^{-1}) respectively. Thermodynamic parameters (ΔG°: -11.42 kJ mol^{-1}, ΔH°: 33.3 kJ mol^{-1}, ΔS°: 145.8 kJ mol^{-1} K^{-1}), also indicated Methyl Orange dye adsorption is feasible, spontaneous and endothermic. Overall, taking into account the excellent efficiency, good regeneration and acceptable performance in real terms, *Asparagus plant*-capped Fe_3O_4NPs can be introduced as a promising absorbent for dyes removal from aqueous solutions.

Keywords: Methyl Orange (MO) dye, Adsorption capacity, Isotherms, Nanoparticles, Kinetic

1. INTRODUCTION

Water is the most important substance for all life on earth and it is also a valuable resource for human civilization [1], approximately 780 million people do not have access to improved quality of water sources, so it is the major worldwide challenge for the 21st century to provide clean and affordable water to human life. Rapid industrialization as well as urbanization helps in releasing heavy metals, dyes, pharmaceuticals, endocrine disruptors, and various pollutants in water bodies [2]. Water is a major route through which metals, dyes and other elements can enter in human body easily due to consumption of contaminated water [3]. Dyes are extensively used for various industries for coloring fabrics, and it is of great importance in creating visual aesthetics. During the past few years, there

*Corresponding author: geramialireza42@gmail.com

has been an increasing concern regarding the residual dye in textiles, as it will be released into the environment. Residual dye is produced when an incomplete or excess of dyes onto textile fiber is incoming out during an aqueous dyeing and washing process [4,5].

Azo dyes are divided according to the presence of azo bonds (–N=N–) in the molecule; these include mono azo, diazo, triazo, etc. [6]. Azo dyes resist the effect of oxidation agents and light, thus they cannot be completely treated by conventional methods of anaerobic digestion. Methyl Orange as shown in (Fig. 1), a well-known azo dye, is used in various industries as redox indicator is widely used by industries [7,8].

Adsorption is a diverse process and is extensively used to remove contaminants from the wastewater. Adsorption is one of the best and simple techniques for the removal of toxic and noxious impurities in comparison to other conventional protocols such as flocculation, membrane filtration, advanced oxidation, ozonation, photo catalytic degradation, and biodegradation [9-12]. Activated carbon is mainly used as an adsorbent in adsorption processes. However, the extensive application of activated carbon in wastewater treatment are limited due to its higher cost [13]. Furthermore, it should be noted that the application of the adsorption process depends largely on the availability of inexpensive adsorbents; the recent initiatives in the adsorption process have inspired the researchers to find available adsorbents and high frequency [14]. The addition of metal oxide nanoparticles to the polymer matrix many benefits exist for adsorption and removal pollutants. Iron nanoparticles including a large surface area, being widely accessible, being stable in an acidic/basic environment, and having a stable structure at high temperatures one of the most widely used nanoparticles is the adsorption process [15]. Hence, it has been extensively used for removal of different chemicals from aqueous solutions. Of these methods, nanomaterial's based adsorbents is highly recommended for dyes pollutants removal [16,17]. The efficient applicability of an adsorption process mainly depends on the physical and chemical characteristics of the adsorbent, which is expected to have high adsorption capacity and to be recoverable and available at economical cost. Currently, various potential adsorbents have been implemented for removal of specific organics from water samples. In this regard, magnetic nanoparticles (MNPs) have been studied extensively as novel adsorbents with large surface area, high adsorption capacity and small diffusion resistance. For instance, they have been used for separation of chemical species such as environmental pollutants, metals, dyes, and gases [18,19]. Iron nanoparticles including a large surface area, being widely accessible, being stable in an acidic/basic environment, and having a stable structure at high temperatures one of the most widely used nanoparticles is the adsorption process [17-19].

In the present work, *Asparagus plant*-capped Fe_3O_4NPs as a novel adsorbent was simply synthesized. Via studying the experimental conditions of pH, contact time, initial (MO) dye concentration, adsorbent dosage and the dye removal percentage, were investigated and optimized. It was shown that the adsorption of (MO) dye follows the pseudo-second-order rate equation. The Langmuir model was found to be applied for the equilibrium data explanation. It was shown through the study of Kinetic models (both pseudo-first-order, pseudo-second-order diffusion models) that the kinetic of adsorption process is controlled by the pseudo-second-order model. The capability of *Asparagus plant*-capped

Fe_3O_4NPs in eliminating of (MO) dye from wastewater treatment was demonstrated by evidences.

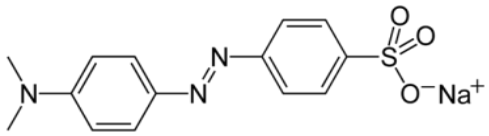

Fig. 1. Chemical structure of Methyl Orange (MO) dye.

2. EXPERIMENTAL

2.1. Chemical and instruments

Methyl Orange (MO) dye (99%), Iron Oxide (%), sodium hydroxide (99%), hydrochloric acid (37%). They were supplied from Merck (Darmstadt, Germany). The morphology of samples was studied by scanning electron microscopy (SEM: KYKY-EM 3200, Hitachi Company, China) under an acceleration voltage of 26kV). The pH/Ion meter (model-728, Metrohm Company, Switzerland, Swiss) was used for the pH measurements. Dyes concentrations were determined using Jasco UV–Vis spectrophotometer model V-530 (Jasco Company, Japan).

2.2. Preparation Asparagus plant-capped Fe_3O_4NPs

Fe_3O_4NPs were prepared by mixing $FeCl_2{\cdot}4H_2O$ (2.74 g), $FeCl_3{\cdot}6H_2O$ (3.11 g) and 0.85 mL concentrated hydrochloric acid into 25 mL deionized water. In the designed method, the synthesis of Fe_3O_4NPs was done by introducing nitrogen gas through a sparer into the solution for oxygen removal. The bubbling of nitrogen gas through the solution protects Fe_3O_4 against critical oxidation and reduces the particles size when compared to synthesis methods without oxygen removal [20].

During the whole process, the solution temperature was maintained at 80°C. After completion of the reaction, the obtained Fe_3O_4NPs were separated from the reaction medium by the magnetic field, then we increased the bath temperature to 90°C. The sediment suspension was stirred for 3 hours. Stirring was stopped and the suspension was placed in the laboratory for 2 hours. The carbon-produced suspensions were prepared from a leaf medlar with an equal weight ratio and after analysis, BET, XRD, FT-IR and SEM were used as adsorbent.

2.3. A typical adsorption experiment

Generally, batch method is currently used in adsorption studies. 250 mL solution having (15 mg/L), concentration of (MO) dye was prepared and the effect of parameters affecting the removal (MO) dye including initial concentration of the ion, pH, dosage sorbent in the range (0.02 to 2.0 g), time intervals (5 to 30 min) were agitated at a constant rate of 200 rpm in a temperature-controlled orbital shaker maintained at 30±1°C was studied in the process. In order to determine the probable amount of (MO) dye onto *Asparagus plant*-capped Fe_3O_4NPs, using a using a double beam UV–vis spectrophotometer (jasco, Model UV–vis V-530, Japan) set at wavelengths 650 nm for (MO) dye as show in (Fig. 2), and the equilibrium concentrations and removal efficiency (%) of the (MO) dye were calculated according to equations (1) and (2), respectively. Meanwhile, all experiments were performed five times and final results were presented as mean values.

$$R\% = \frac{C_0 - C_e}{C_0} \times 100 \quad (1)$$

$$q_i = \frac{V(C_0 - C_e)}{M} \times 100 \quad (2)$$

C_0 (mg/L) in the formula refers to the initial (MO) dye concentration and C_e (mg/L) represents the equilibrium (MO) dye concentration in aqueous solution. V (L) shows the solution volume and W (g) signifies the mass adsorbent [21,22].

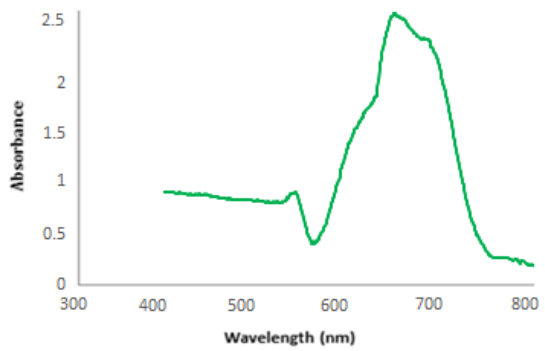

Fig. 2. Absorption spectra of (MO) dye onto *Asparagus plant*-capped Fe_3O_4NPs.

3. RESULTS AND DISCUSSION

3.1. The evaluation special surface of Asparagus plant-capped Fe_3O_4NPs *as an adsorbent*

The Brunauer–Emmett–Teller (BET) analysis was used for determination of surface area of the *Asparagus plant*-capped Fe_3O_4NPs by N_2 adsorption before and after (MO) dye adsorption. The decrease of surface area indicate that (MO) dye is almost in almost all *Asparagus plant*-capped Fe_3O_4NPs pores after absorption [23]. The adsorption capacity with an increase in the number of adsorbed Fe_3O_4NPs, the relative partial pressure range on the adsorption isotherms gradually decreases. This is because the Fe_3O_4NPs, in the composite spread into *Asparagus plant* channels, made the channels narrow and the pore volume decrease. The gradual decrease of BET specific surface area indicates that the Fe_3O_4NPs, and has entered the *Asparagus plant* pores rather than adsorbed on the outer surface of the *Asparagus plant*. By comparing the pore size distribution of the samples, it can be seen that with the increase of gradually the increase of the number of adsorbed Fe_3O_4NPs, the most probable pore diameter is gradually reduced. This is because when the Fe_3O_4NPs, was introduced into the *Asparagus plant*, channels, the most probable pore diameter reduced, indicating that the Fe_3O_4NPs, entered the *Asparagus plant* channels in the (Table.1).

FT-IR analysis - The FT-IR spectra of *Asparagus plant*-capped Fe_3O_4NPs in the 400–4000 cm^{-1} wave number range, as demonstrated in Fig. 3, the FT-IR spectrum of *Asparagus plant*-capped Fe_3O_4NPs presents clear peak at 877 cm^{-1} related to Fe–O. The absorption band at 1635 and 1532 cm^{-1} is due to the O–H bending vibration from the water molecules adsorbed into *Asparagus plant*-capped Fe_3O_4NPs (Fig. 3). The novel emerging signal at 3350 cm^{-1} can be attributed to –OH stretching [24].

XRD analysis - Different X-ray emission peaks are *Asparagus plant*-capped Fe_3O_4NPs shown in (Fig. 4). The signal at $2\theta = 24.7^{\circ}$ (311) is ascribable to diffractions and reflections from the carbon atoms. The positions of diffraction peaks are in agreement with the standard samples of *Asparagus plant*-capped Fe_3O_4NPs [25].

Surface morphology - The morphological properties of *Asparagus plant*-capped Fe_3O_4NPs was investigated by FE-SEM and is exhibited in (Fig. 5), *Asparagus plant*-capped Fe_3O_4NPs after surface modification came to be uneven, bigger and agglomerate**.** It can be seen that the particles are mostly spherical with the various size. Based on the particle size distribution, we obtained the average particle size in the range of 45-65 nm very close to those determined by XRD analysis [26].

Table 1. Characteristics of the *Asparagus plant*-capped Fe_3O_4NPs.

Parameter	Bulk density (g/mL)	Loss of mass on ignition	Surface area (m^2/g)	Particle size range (µm)
Value	0.607	0.6235	250.0	45.0-250.0

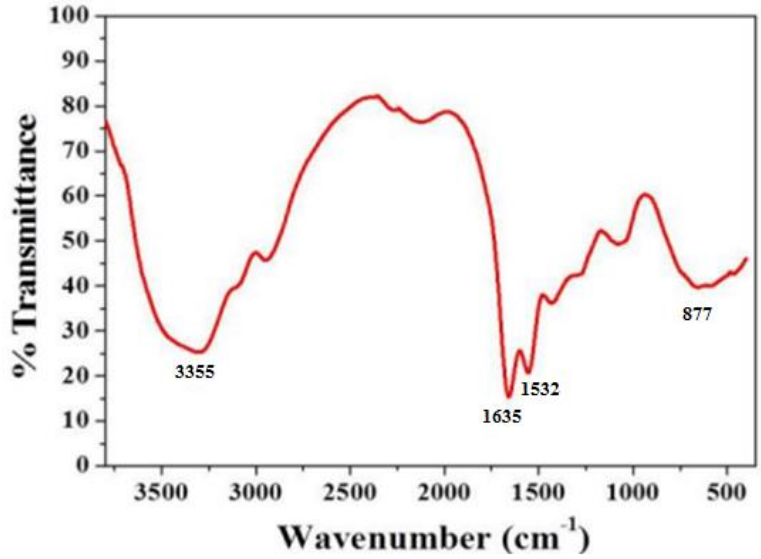

Fig. 3. FT-IR transmittance spectrum of the prepared *Asparagus plant*-capped Fe_3O_4NPs.

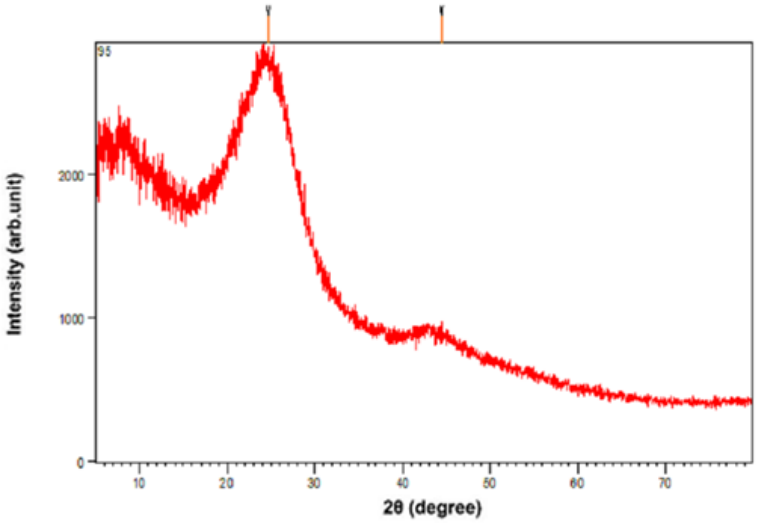

Fig. 4. X-ray diffraction of *Asparagus plant*-capped Fe_3O_4NPs.

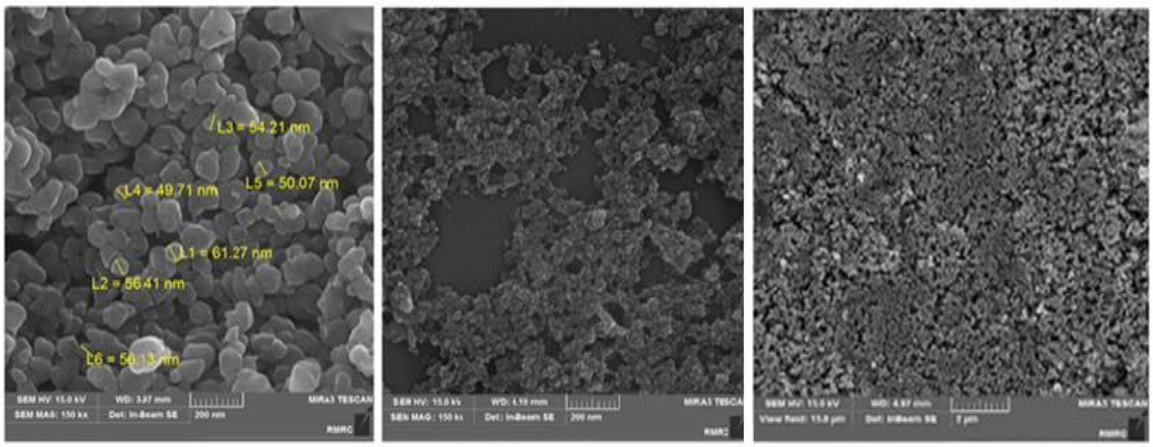

Fig. 5. The (SEM) image of the prepared *Asparagus plant*-capped Fe_3O_4NPs.

3.2. Impact of pH on the adsorption

The impact of pH value in the adsorption process is considerable. The deletion of (MO) dye onto sorption *Asparagus plant*-capped Fe_3O_4NPs as a function of pH by varied sorbent is shown in (Fig. 6). To control optimum pH for the highest deletion of (MO) dye, the measurement of equilibrium adsorption of (MO) dye was done at varied pH levels from 1.0 to 8.0 through adjusting the initial (MO) dye concentrations at 15 mg/L and the summary of the obtained outcomes are displayed [26, 27]. The highest deletion percentages of (MO) dye was procured at pH 7.0. Abatement in (MO) dye deletion at pH <7 happened due to competition of (MO) dye with H^+. Additionally in highly acidic pH, sharp concentration of H^+ set the scene for protonation of nitrogen atoms on the surface of adsorbents and provoked the reduction of interaction with (MO) dye and surface of adsorbents. Both reasons of precipitation of hydroxide and conversion of (MO) dye provoked the reduction in (MO) dye deletion at pH >7. This phenomenon obstructed the access of (MO) dye to adsorption sites and culminated in less adsorption of (MO) dye onto sorption *Asparagus plant*-capped Fe_3O_4NPs [28].

3.3. Impact of the dosage of sorbent

The sorption efficiency for (MO) dye as a function of sorbent dosage was investigated. The percentage of the dyes sorption steeply increases with the sorbent loading up to 0.1 g in (Fig. 7). This result can be explained by the fact that the sorption sites remain unsaturated during the sorption reaction, whereas the number of sites available for sorption site increases by increasing the sorbent dose [29]. The maximum sorption was attained at sorbent dosage, 0.1 g. Therefore, the optimum sorbent dosage was taken as 0.1 g for further experiments. This can be explained by when the sorbent ratio is small, the active sites for binding dye on the surface of *Asparagus plant*-capped Fe_3O_4NPs is less, so the sorption efficiency is low. As the sorbent dose increased, more active sites to bind (MO) dye, thus it results an increase in the sorption efficiency until saturation [30].

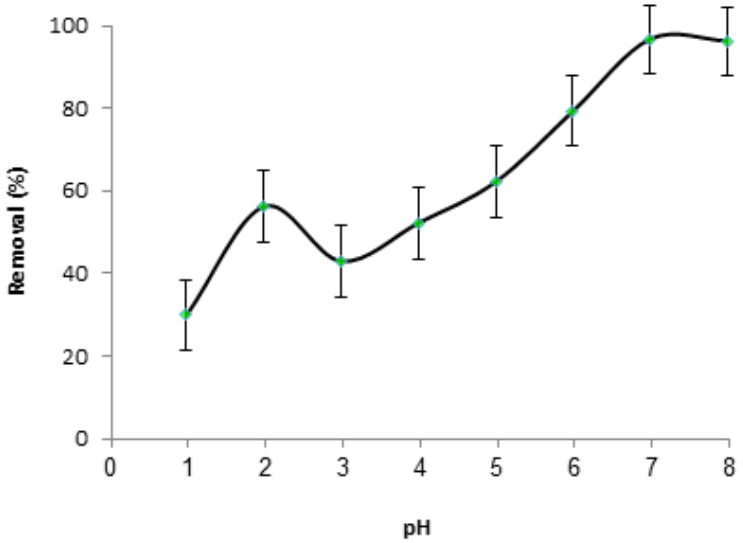

Fig. 6. Impact of initial solution pH on the adsorption amount of (MO) dye onto *Asparagus plant*-capped Fe_3O_4NPs [(MO) dye = 15 mg L^{-1}; dosage sorbent = 0.1 g; time = 20.0 min].

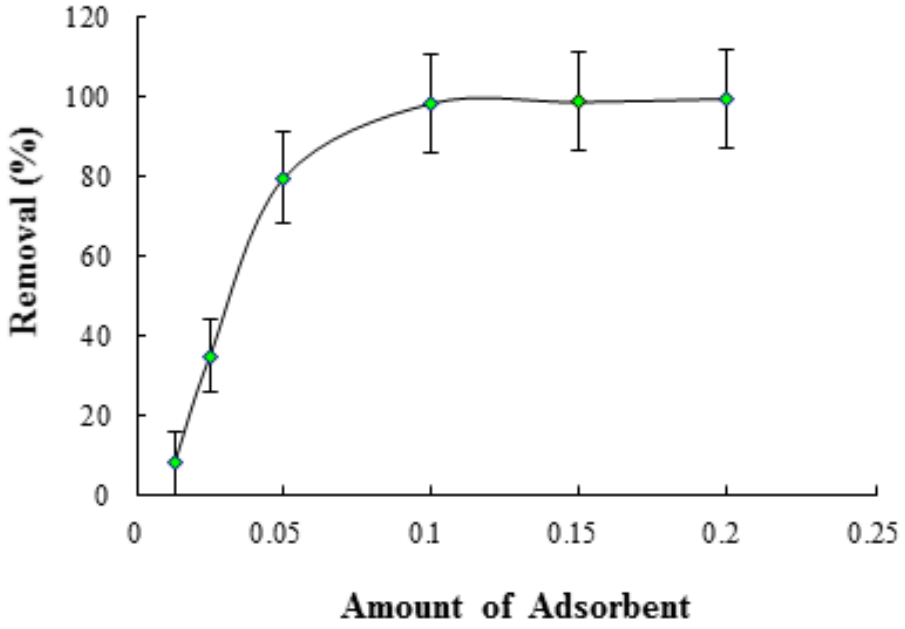

Fig. 7. Impact of dosage sorbent on the adsorption amount of (MO) dye [(MO) dye = 15 mg L^{-1}; pH =7.0; time = 20.0 min].

3.4. Impact of the contact time on the adsorption

Since the rate of sorption is considered crucial for designing batch bio sorption experiments, thus, the impact of contact time on the sorption of (MO) dye by *Asparagus plant*-capped Fe_3O_4NPs was examined. A considerable increase in the sorption of (MO) dye was observed for the contact time of 20 min. The impact of initial dye concentration (MO) dye sorption by a *Asparagus plant*-capped Fe_3O_4NPs was scrutinized in batch experiments applying 5 at 30 min contact time, pH value 5 for (MO) dye, 0.1 g adsorbent dose and the constant temperature 300.15 K [31,32]. With an increase in the initial concentration of (MO) dye, a gradual boost in the equilibrium uptake of the sorbent was observed. The elevation of sorption yield along with the elevation in dye concentration can probably be a result of higher interaction between the (MO) dye and sequestering sites of the sorbent shown in (Fig. 8).

3.5. Impact of temperature

To study the effects of temperature on the adsorption of (MO) dye into *Asparagus plant*-capped Fe_3O_4NPs the experiments were performed at temperatures from 283.15 to 333.15 K. (Fig. 9), shows the influence of temperature of (MO) dye into *Asparagus plant*-capped Fe_3O_4NPs is shown in (Fig. 9). As it can be seen, the adsorption (MO) dye into *Asparagus plant*-capped Fe_3O_4NPs of the process decreases with the temperature increasing. This may be come from the fact that the adsorption process may be endothermic one [33].

3.6. Impact of concentration on the adsorption of (MO) dye

For this purpose, in a series of similar experiments, 50 ml of (MO) dye solution with concentrations different (mg/L), and

0.1 g of *Asparagus plant*-capped Fe_3O_4NPs, pH 7 and other variables for: 20.0 minutes at 200 rpm, respectively, stirred at room temperature to adsorb dye on the modified activated carbon Be done with nanoparticles. The major adsorption of dye takes place at low concentrations and with increasing concentration, the percentage of adsorption decreases. Although with increasing initial concentration, the amount of adsorbed dye increases, but the percentage of its removal decreases. The results are presented in (Fig.10) [34].

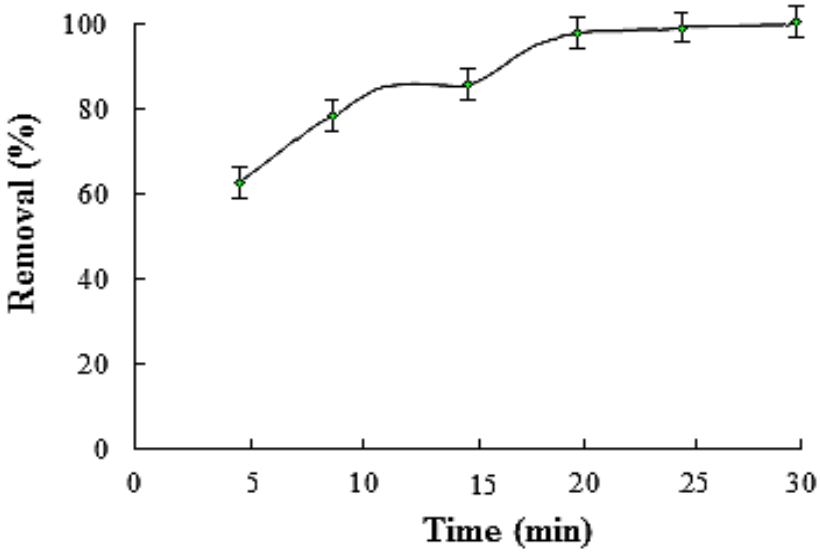

Fig. 8. Impact of contact time on the adsorption of (MO) dye onto *Asparagus plant*-capped Fe_3O_4NPs [(MO) dye = 15 mg L^{-1}; pH =7.0; dosage sorbent = 0.1 g].

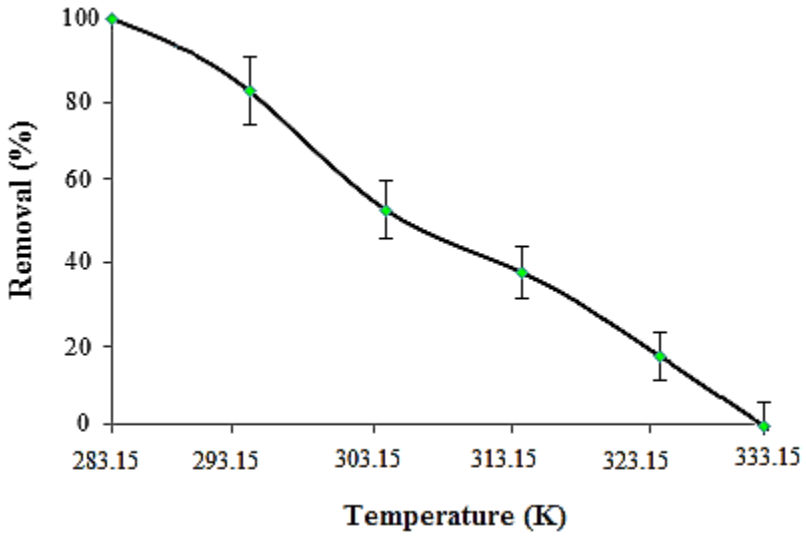

Fig. 9. Impact of temperature on the sorption of (MO) dye into *Asparagus plant*-capped Fe_3O_4NPs [(MO) dye conc =15 mg L^{-1}; pH =7; adsorbent dose =0.1g; time =20 min; stirring speed =200 rpm].

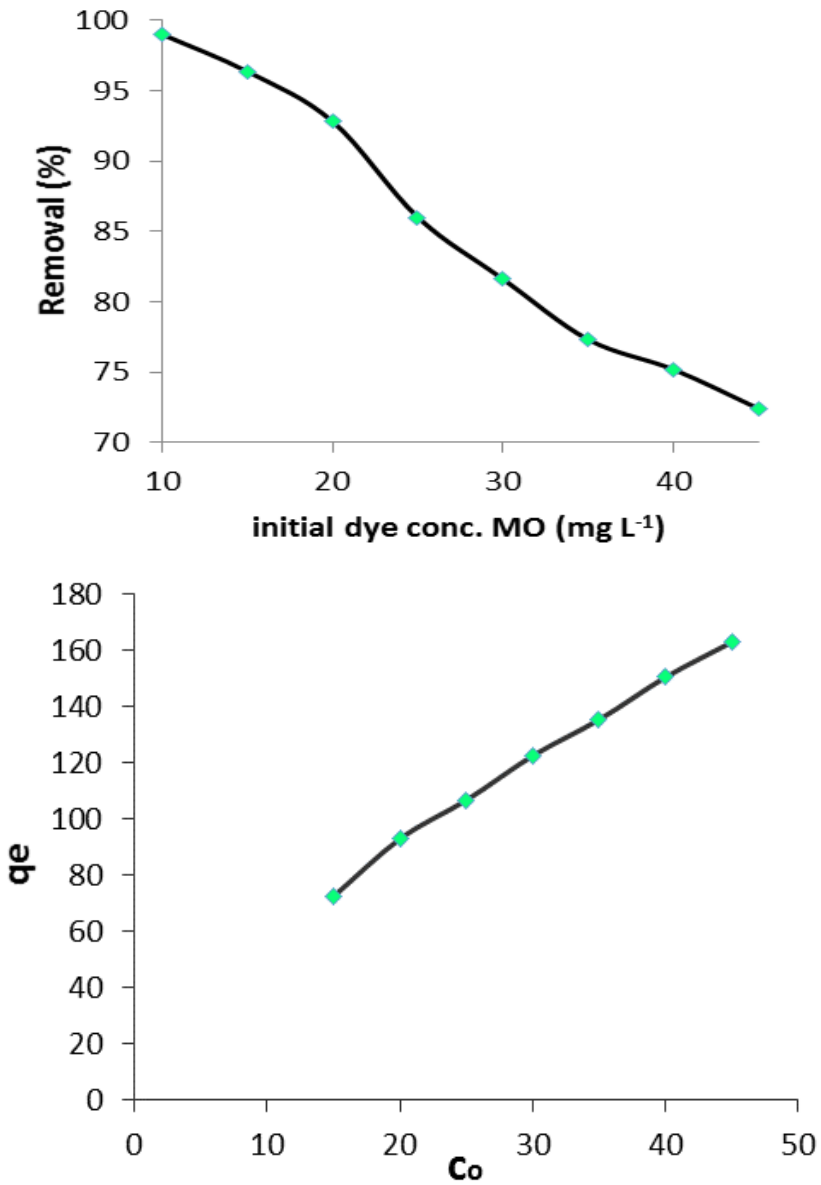

Fig. 10. Impact of concentration on the adsorption of (MO) dye [pH = 7; adsorbent dose = 0.1g; time = 20 min; stirring speed = 200 rpm].

3.7. Adsorption isotherms

Equilibrium adsorption analysis is important to find out the adsorption levels at a specific adsorbate concentration and to underpin the further types of adsorption followed. The experiments were conducted by varying the contact time and evaluating the equilibrium adsorbate concentration (C_e) and equilibrium adsorption capacity (q_e). The obtained data were analysed based on the established adsorption isotherm models. The theoretical details are given in Supplementary Information [35,36].

Langmuir adsorption isotherm: In this model, there is no interaction among adsorbed molecules and adsorption process happens on homogeneous surfaces, showed in below equation [36]:

$$\frac{C_e}{q_e} = \frac{1}{K_L q_{\max}} + \frac{1}{q_{\max}} C_e \qquad (3)$$

In relation (3) q_m: is the value of monolayer adsorption capacity in Langmuir model and K_L: constant value of Langmuir (mg/L). Increasing the amount of adsorbent caused a considerable increase in the adsorbed ions amounts (Fig. 11a).

Freundlich isotherm model is the more for the adsorption of components dissolved in a liquid solution, it is assumed that:

First, the adsorption is monolayer and chemical, and second, the energy of the adsorption sites is not the same, i.e. the adsorbent surface is not uniform [37]:

$$\ln q_e = \ln K_F + \frac{1}{n}\ln C_e \quad (4)$$

K_F and n are experimental constants where k_F is in terms of $((mg)^{1-n}\ L^n/g)$ and is proportional to the adsorption capacity, and n is a unit less quantity and shows the intensity of adsorption with a range between 0.1 to 1.0. Calculation of K_F and adsorption capacity in Freundlich model shown in (Fig. 11b).

The isotherm model of Temkin (Fig. 11c), was employed to evaluate indirect adsorbate/adsorbate base on following equation:

$$q_e = \frac{Rt}{b} ln\ K_T + \frac{RT}{b} lnC_e \quad (5)$$

In this model as mentioned above, R, b, t, K_T and T are the universal gas constant (8.314 J/mol. K), Temkin constant, the heat of the adsorption (J/mol), the binding constant at equilibrium (L/mg) and absolute temperature (K) [38].

Dubinin–Radushkevich (D-R) isotherms: For investigated the nature of adsorption, this model is used. The linear form of this model expressed by the following equation: [39].

$$Lnq_e = lnq_m - \beta\varepsilon^2 \quad (6)$$

Where β is the activity coefficient related to mean sorption energy. (mol^2 / kJ^2), and ε is the Polanyi potential that can be calculated from bellow equation:

$$\varepsilon = RTln(1+1/Ce) \quad (7)$$

The slope of the plot of ln q_e versus ε^2 gives B and its intercept yields the Q_s value shown in (Fig. 11d). The linear fit between the plot of C_e/q_e versus C_e and calculated correlation coefficient (R^2) for Langmuir isotherm model shows that the dye removal isotherm can be better represented by Langmuir model (Table. 2). This confirms that the adsorption of dye takes place at specific homogeneous sites as a monolayer on to the *Asparagus plant*-capped Fe_3O_4NPs.

The chi square (X^2) tests were adopted to determine the suitability of the isotherm model with respect to the experimental data. The X^2 equation is as follows:

$$X^2 = \sum_{i=1}^{m} \frac{(qe,exp - qe,calc)^2}{qe(exp)} \quad (7)$$

Where qe (mgg^{-1}) is the experimental equilibrium capacity and qe, m (mgg^{-1}) is the equilibrium capacity obtained from the model [37].

3.8. Further discussion about Langmuir isotherm

Investigation about the adsorption uptake of (MO) dye was done for initial concentration range from 5 to 40 mg/L and exhibited in (Fig. 12). The essential features of a Langmuir isotherm can be expressed in terms of a dimensionless constant separation factor or equilibrium parameter, R_L that is used to predict if an adsorption system is favorable or unfavorable [40]. Langmuir isotherm can be criticized in terms of a dimensionless constant separation factor or equilibrium parameter, R_L which is used to predict if the isotherm model favorable or not. The R_L factor is defined as follows:

$$R_L = \frac{1}{1 + K_L C_0} \quad (9)$$

The values of R_L can illustrate the shape of the isotherm to be either unfavorable (R_L>1), linear (R_L=1), favorable (0<R_L<1) or irreversible (R_L=0). The plot of the calculated R_L values versus initial concentration of MO dye is shown in (Fig. 12), indicating that the Langmuir adsorption isotherm is fairly suitable for MO adsorption onto *Asparagus plant*-capped Fe_3O_4NPs adsorbent.

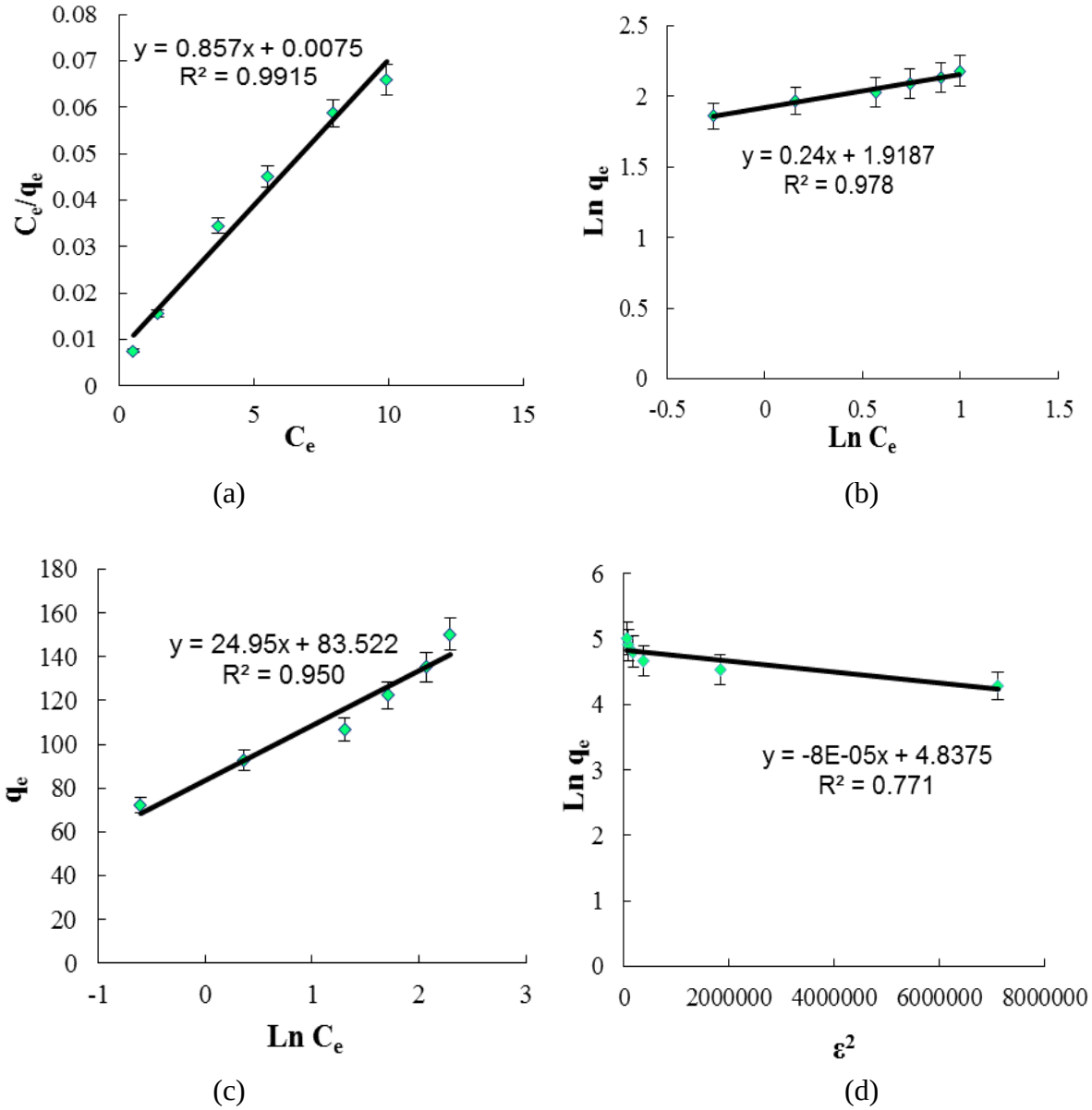

Fig. 11. (a) Langmuir isotherm (b) Frendlich isotherm (c) Temkin isotherm (d) Dubinin-Radushkevich isotherm on the sorption quantity of (MO) dye *Asparagus plant*-capped Fe_3O_4NPs [(MO) dye = 15 mg L^{-1}; pH = 7; adsorbent dose = 0.1g; time = 20 min; stirring speed = 200 rpm].

Table 2. Various isotherm constants and correlation coefficients calculated for the adsorption of (MO) dye by *Asparagus plant*-capped Fe_3O_4NPs [(MO) dye conc = 15 mg L^{-1}; pH = 7; adsorbent dose = 0.1 g; time = 20 min; stirring speed = 200 rpm].

Isotherm	Parameters	R% (MO)
Langmuir	q_m (mgg^{-1})	167.7
	K_L (Lmg^{-1})	0.857
	R^2	0.9915
	$\sum x^2$	11.87
Freundlich	1/n	0.24
	K_F $(mg)^{1-n} L^n/g$	82.8
	R^2	0.978
	$\sum x^2$	711.93
Temkin	B_T ($J.mol^{-1}$)	24.95
	K_T ($L\ mg^{-1}$)	28.05
	R^2	0.950
Dubinin–Radushkevich (D–R)	q_m (mgg^{-1})	125.9
	B	8E-05
	E (J/mol) = $1/(2B)^{1/2}$	2500
	R^2	0.771

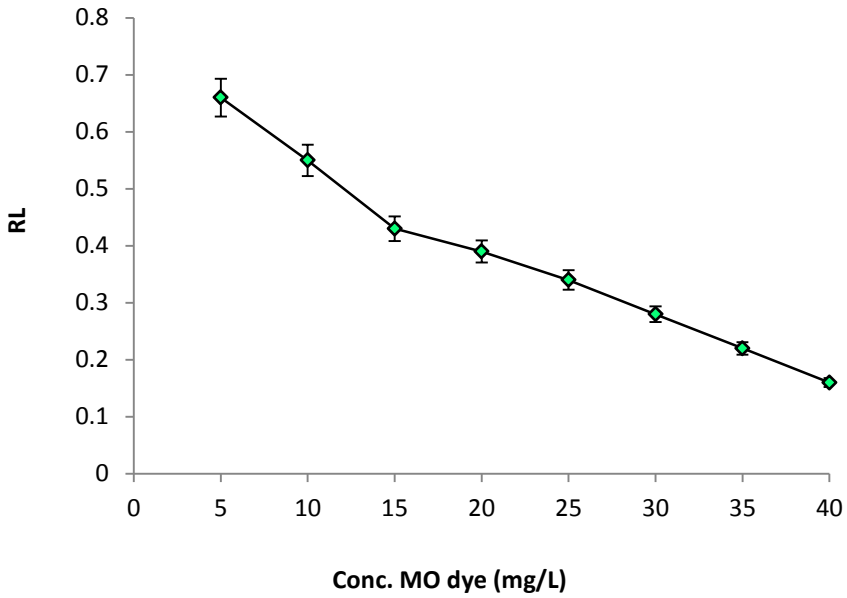

Fig. 12. Plot of R_L versus C_0, that Langmuir isotherm is favorable for representing the experimental data of the (MO) dye by *Asparagus plant*-capped Fe_3O_4NPs [(MO) dye = 15 mg L^{-1}; adsorbent dose = 0.1 g; pH = 7; contact time = 20 min; stirring speed = 200 rpm].

3.9. Adsorption kinetics

Adsorption kinetics is one of the most important factors which represent the adsorption efficiency of *Asparagus plant*-capped Fe_3O_4NPs. The theoretical details are given in Supplementary [40,41].

The quasi-first-order kinetic model formula is:

$$\ln(q_e - q_t) = \ln q_e - \frac{k_1}{2.303} t \qquad (10)$$

The quasi-second-order dynamic model formula is:

$$\frac{t}{q_t} = \frac{1}{k_2 q_e^2} + \frac{t}{q_e} \qquad (11)$$

The slopes and intercepts of plots of t/q vs.t were used to calculate the second-order rate constant k_2, t and qe. Generally, these constants are used to predict the adsorption behavior, which is inconsistent with rate-controlling step in adsorption mechanism. The obtained kinetic data for adsorption of (MO) dye onto *Asparagus plant*-capped Fe_3O_4NPs an adsorbent were examined as shown in (Fig. 13) [42,43].

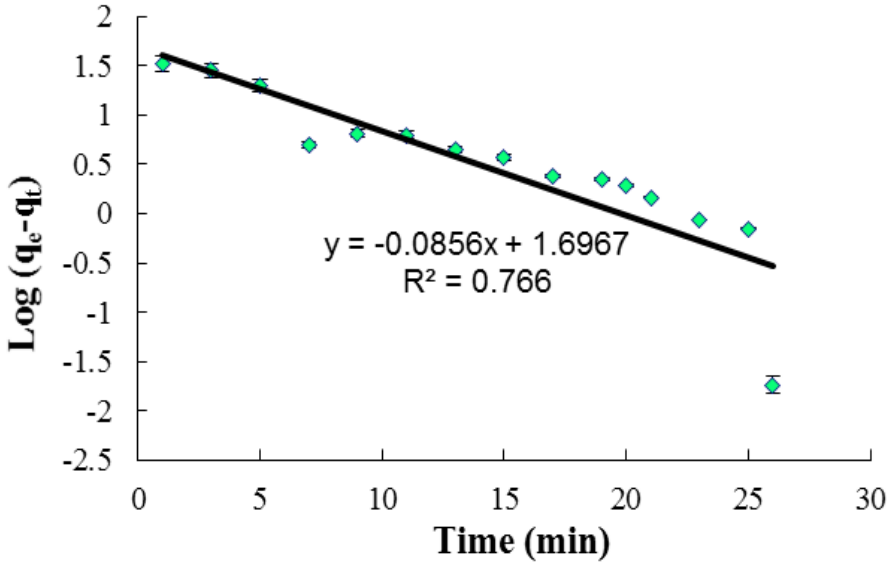

(a)

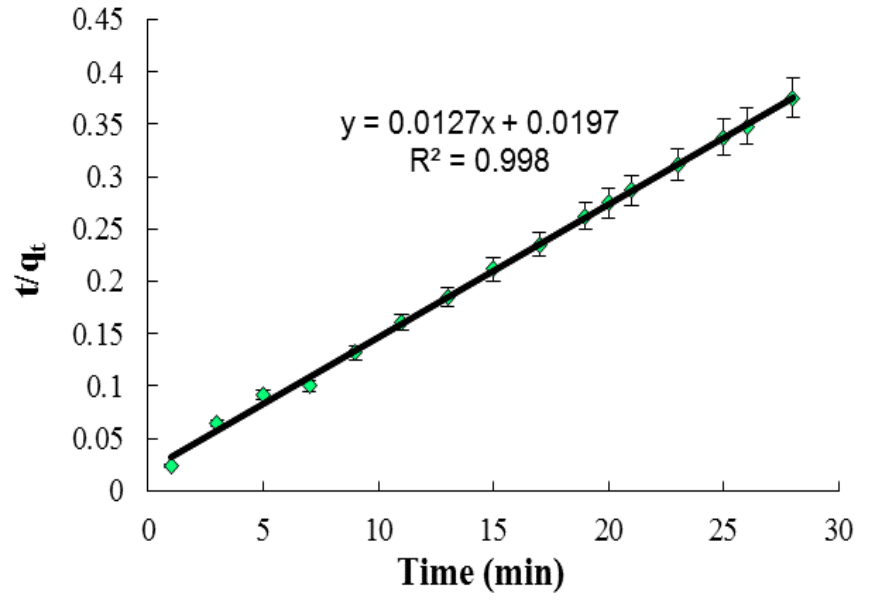

(b)

Fig. 13. (a) pseudo-first-order kinetic model (b) pseudo-second-order kinetic model for the adsorption of (MO) dye onto *Asparagus plant*-capped Fe_3O_4NPs [(MO) dye conc = 15 mg L^{-1}; pH = 7; adsorbent dose = 0.1 g; time = 20 min; stirring speed = 200 rpm].

Table 3. Kinetic parameters for the adsorption for the adsorption of (MO) dye onto *Asparagus plant*-capped Fe_3O_4NPs [(MO) dye conc = 15 mg L^{-1}; pH = 7; adsorbent dose = 0.1 g; time = 20 min; stirring speed = 200 rpm].

Models Kinetics	parameters	R% MO
Pseudo-first-order	k_1 (1/min)	0.205
	qe (mgg^{-1})	65.52
	R^2	0.766
Pseudo-second-order	$K_2\times10^{-3}$ (1/min)	6.1
	qe (mgg^{-1})	83.33
	R^2	0.998
	H	43/478
q_e (exp)		74.72

3.10. Adsorption thermodynamics

Temperature is one of the most important factors in ions removal efficiency by focusing on change in nature of the reaction (exothermic or endothermic) to reveal spontaneous and non-spontaneous reaction. Thermodynamic parameters can be using the Eqs. (12) and (13) [44].

$$\Delta G^{\circ} = -RT \ln K_{ad} \quad (12)$$

$$\ln K_{ad} \frac{\Delta H^{\circ}}{RT} + \frac{\Delta S^{\circ}}{R} \quad (13)$$

Where, T is the temperature in Kelvin, R the gas constant (8.314 J. mol^{-1} K^{-1}), ΔS° and ΔH° values can also be determined from the slope and intercept of the plot of Ln K^0 values 1/T, respectively (Fig. 14 and Table. 4). The Gibbs free energy (ΔG^0 degree of spontaneity of the adsorption process and the low values reflect an energetically favorable adsorption process. The negative value of (ΔH°) confirms that the sorption process was exothermic in nature and a given amount of heat is evolved during the binding of (MO) dye onto *Asparagus plant*-capped Fe_3O_4NPs the surface of adsorbent. The highly negative ΔS^0 values indicate significant decrease in the degree of randomness at solid/liquid interface during the sorption process [45,46].

3.11. Desorption

Close scrutiny of desorption is beneficial in exploring the possibility of recycling the adsorbents. Desorption of (MO) dye by HCl is exhibited in (Fig. 15). A range from 0.1 to 0.5 M concentrations of HCl solutions was put to the test for eliminating (MO) dye from the adsorbent. Based on the obtained results, it becomes evident that the maximum desorption of (MO) dye was (95.0 %) from *Asparagus plant*-capped Fe_3O_4NPs by HCl (0.25 M). Thenceforth, no competition for exchange sites was observed between (MO) dye and H^+ ions and consequently (MO) dye were released into the solution.

3.12. Comparison with other adsorbents for removal (MO) dye

Many adsorbents have been used to adsorb (MO) dye and achievement of waste water treatment and their operational parameters were compared. This comparison was carried out by the maximum adsorption capacity (q_{max}) obtained for removal (MO) dye and respective results are reported in (Table. 5).

4. CONCLUSION

The selection of *Asparagus plant*-capped Fe_3O_4NPs as an efficacious adsorbent for the deletion of (MO) dye from aqueous solutions has been scrutinized. In this current article, the applicability of *Asparagus plant*-capped Fe_3O_4NPs as an available, useful, and affordable material

for deleting (MO) dye from aqueous media has been confirmed. The desired values of the pH, adsorbent dosage, (MO) dye concentration, and contact time were found to be 7, 0.1 g, 15 mg L^{-1}, and 20.0 min for adsorption of (MO) dye into *Asparagus plant*-capped Fe_3O_4NPs. The kinetics and isotherm studies proved the appropriateness of the pseudo second-order and Langmuir isotherm models for the kinetics and isotherm of the adsorption of (MO) dye on the adsorbent. Since almost 99.0% of (MO) dye was deleted with ideal adsorption capacities of 167.7 mgg^{-1} for (MO) dye. Thermodynamic parameters ($\Delta G°$: -11.42 kJ mol^{-1}, $\Delta H°$: 33.3 kJ mol^{-1}, $\Delta S°$: 145.8 kJ/mol K) for both (MO) dye are positive, which confirm the endothermic nature of the sorption process. According to the findings of this study, *Asparagus plant*-capped Fe_3O_4NPs could be employed as a reusable adsorbent and would be an economically viable option that can lead to wastewater treatment advancement and high-quality treated effluent.

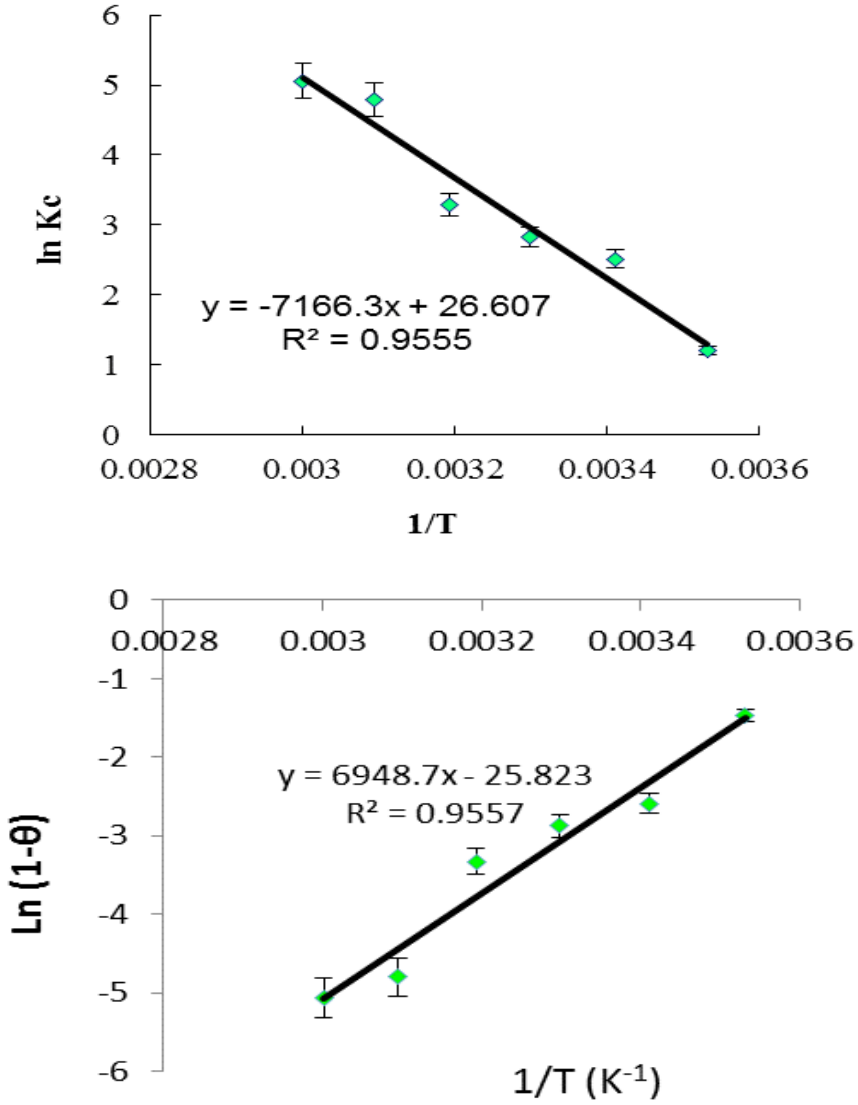

Fig. 14. (a) Plot of ln Kc vs. 1/T (b) Ln (1-Θ) vs. 1/T for estimating thermodynamic parameters.

Table 4. The thermodynamic parameters for the adsorption of (MO) dye onto *Asparagus plant*-capped Fe_3O_4NPs [(MO) dye =15.0 mg L^{-1}; pH =7.0; dosage sorbent = 0.1 g; time = 20.0 min].

Dyes (mg/L)	T (^{O}K)	value of ΔG^{o}(kJ/mol)	value of ΔH^{o}(kJ/mol)	value of ΔS^{o} (k/mol K)
Methyl Orange (MO) dye (15 mg/L)	283.15	-11.42	33.3	145.8
	293.15	-36.80		
	303.15	-60.93		
	313.15	-63.62		
	323.15	-78.62		
	333.15	-85.64		

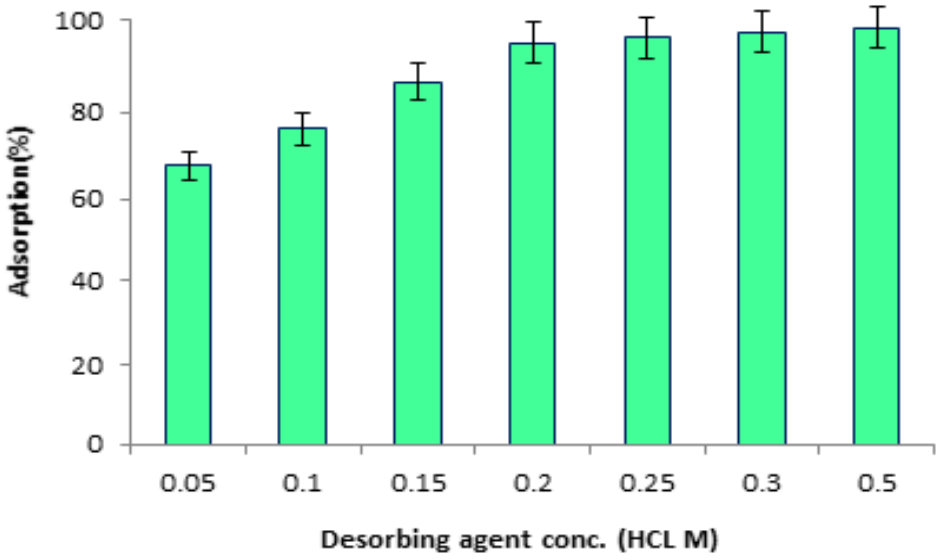

Fig. 15. Desorption plot of the (MO) dye by HCl [(MO) dye = 15.0 mg L^{-1}; pH =7.0; dosage sorbent = 0.1 g; time = 20.0 min].

Table 5. Comparison of results for this work with other reported.

Dye	Adsorbent	Dosage sorbent	pH	Time	Adsorption capacity	References
(MO) dye	sheep manure biochar	0.6 g	4.0	60 min	42.513 to 45.563 mgg^{-1}	[6]
(MO) dye	chicken manure biochar	0.5 g	6.0	120 min	39.47 mgg^{-1}	[9]
(MO) dye	Graphene oxide	0.5 g	3.0	100 min	16.83 mgg^{-1}	[21]
(MO) dye	Cork powder	0.5 g	2.0	240 min	16.66 mgg^{-1}	[29]
(MO) dye	Fe_2O_3–BC composite	0.1 g	8.0	30 min	20.53 mgg^{-1}	[40]
(MO) dye	Fe_3O_4 –AC nanocomposites	1.0 g	4.5	60 min	32.63 mgg^{-1}	[47]
(MO) dye	*Asparagus plant*-capped Fe_3O_4NPs	0.1 g	7.0	20 min	167.7 mgg^{-1}	Present study

Acknowledgement

The authors gratefully acknowledge partial support of this work by the Islamic Azad University, Branch of Dashtestan, Iran.

References

[1] L. P. Lingamdinne, J. R. Koduru, R. R. Karri, J. Environ. Manage. 231, 622 (2019).

[2] R. Senthilkumar, D. M. Reddy Prasad, L. Govindarajan, K. Saravanakumar, B.S. Naveen Prasad, Separa. Sci. Technol. 54(15), 2351 (2019).
[3] S. A. Haji Azaman, A. Afandi, B. H. Hameed, A.T. Mohd Din, J. Appl. Sci. Eng. 21(3), 317 (2018).
[4] M. Venkata Ratnam, C. Karthikeyan, K. Nagamalleswara Rao, V. Meena, J. Mater. Today Proceed. 26(2), 2308 (2020).
[5] A. Reghioua, D. Barkat, A. H. Jawad, A. S. Abdulhameed, A. A. Al-Kahtani, A. A. Al-Othman, J. Environ. Chem. Eng. 9, 105166 (2021).
[6] J. Hosseini, H. Aghaie, M. Ghaedi, Orient. J. Chem., 30(4), 1883 (2014).
[7] M. A. Salam, S. A. Kosa, A. A. Al-Beladi, J. Mol. Liquid. 241, 469 (2017).
[8] Y. Lu, J. Chen, Y. Bai, J.Gao, M. Peng, J. Environ. Stud. 28(5), 3791 (2019).
[9] J. Yu, X. Zhang, D. Wang, P. Li, J. Int. Assoc. Water Pollut. Res. 77(5), 1303 (2018).
[10] M. Abniki, A. Moghimi, Micro Nano Lett. 16, 455 (2021).
[11] A. Dalvand, N. Golchinpoor, S. S. Hosseini, E. Gholibegloo, M. R. Ganjali, M. Khazaei, A.H. Mahvi, H. Kamani, Environ. Sci. Pollut. Res. 23, 16396 (2016).
[12] J. H. Park, J. J. Wang, R. Xiao, R. D. DeLaune, D. C. Seo, Bioresource. Technol. 249, 368 (2018).
[13] A. M. Vargas, A. C. Martins, V. C. Almeida, Chem. Eng. J. 195, 173 (2012).
[14] T. M. Coelho, E. Vidotti, M. Rollemberg, A. Medina, M. Baesso, N. Cella, A. Bento, Talanta. 81, 202 (2010).
[15] G. Kiani, M. Dostalia, A. Rostami, A.R. Khataee, J. Appl. Clay Sci. 54, 34 (2011).
[16] M. Ishaq, K. Saeed, I. Ahmad, S. Sultan, S. Akhtar, Iran. J. Chem. Chem. Eng. 33, 53 (2014).
[17] A. Reghioua, D. Barkat, A. H. Jawad, A. S. Abdulhameed, M. R. Khan, J. Sustaina. Chem. Pharm. 20, 100379 (2021).
[18] Z. Jafari Harandi, Sh. Ghanavati Nasab, A. Teimouri, Int J Environ Anal Chem. 99(6), 568 (2019).
[19] F. Marahel, B. Mombeni Goodajdar, N. Basri, L. Niknam, A. A. Ghazali, Iran. J. Chem. Chem. Eng. 40(6), 1 (2021). doi: 10.30492/IJCCE.2021.527025.4636.
[20] R. Manohar, V. S. Shrivastava, J. Mater. Environ. Sci. 6, 11 (2015).
[21] D. Robati, B. Mirza, M. Rajabi, O. Moradi, I. Tyagi, S. Agarwal, V.K. Gupta, Chem. Eng. J. 284, 687 (2016).
[22] N. N. Abd Malek, A. H. Jawad, A. S. Abdulhameed, K. Ismail, B.H. Hameed, Int. J. Biolog. Macromolecules. 146, 530 (2020).
[23] H. S. Ghazi Mokri, N. Modirshahla, M. A. Behnajady, B. Vahid, Int. J. Environ. Sci. Technol. 12, 1401 (2015).
[24] S. Bagheri, H. Aghaei, M. Ghaedi, A. Asfaram, M. Monajemi, A. A. Bazrafshan, Ultrasonics – Sonochemistry. 41, 279 (2018).
[25] M. Naushad, G. Sharma Zeid, A. Alothman, J. Clean. Production. 241, 112863 (2019).
[26] A. Dehghanpoor Frashah, S. Hashemian, F. Tamadon, Eur. J. Anal. Chem. 15, 32 (2020).
[27] F. Maghami, M. Abrishamkar, B. Mombeni Goodajdar, M. Hossieni, Desal. Water Treat. 223, 388 (2021).
[28] M. Ghaedi, S. Hajati, B. Barazesh, F. Karimi, G. Ghezelbash, J. Ind. Eng. Chem. 19, 227 (2013).
[29] F. Krika, F. Benlahbib, Desal. Water Treat. 53, 3711 (2015).

[30] W. P. Utomo, E. Santoso, G. Yuhaneka, A.I. Triantini, M.R. Fatqi, M.F. Hudadan, N. Nurfitria, J. Kimia Chem. 13, 104 (2019).
[31] M. Ghaemi, G. Absalan, L. Sheikhian, J. Iran. Chem. Soc. 11, 1759 (2014).
[32] S. Shariati, M. Faraji, Y. Yamini, A.A. Rajabi, Desalination. 270, 160 (2011).
[33] A. H. Jawad, A. S. Abdulhameed, M. S. Mastuli, J. Taibah, Univ. Sci. 14(1), 305 (2020).
[34] A. Achmad, J. Kassim, T. Kim Suan, J. Phys. Sci. 23, 1 (2012).
[35] R. Mahini, H. Esmaeili, R. Foroutan, Turk. J. Biochem. 24, 1 (2018).
[36] C. Arora, S. Soni, S. Sahu, J. Mittal, P. Kumar, P.K. Bajpai, J. Mol. Liquids. 284, 373 (2019).
[37] Y. Yang, Y. Xie, L. Pang, M. Li, X. Song, J. Wen, H. Zhao, Langmuir. 29, 10727 (2013).
[38] S. Hajati, M. Ghaedi, B. Barazesh, F. Karimi, R. Sahraei, A. Daneshfar, A. Asghari, J. Ind. Eng. Chem. 20, 2421 (2014).
[39] Z. Zubair, I. Ihsanullah, N. Jarrah, A. Khalid, M. S. Manzar, T. S. Kazeem, M. A. Al- Harthi, J. Mol. Liquids. 249, 254 (2018).
[40] Sh. Bouroumand, F. Marahel, F. Khazali, Desal. Water Treat. 223, 388 (2021).
[41] N. Chaukura, E.C. Murimba, W. Gwenzi, J. Appl. Water Sci. 7(5), 2175 (2017).
[42] D. Wang, H. Guo, Y. Li, Z. Wang, F. Shen, Chinese J. Environ. Eng. 10(9), 5172 (2016).
[43] M. Hubbe, S. Azizian, S. Douven, A Review. Bio Resources. 14(3), 7582 (2019).
[44] A. H. Jawad, A.S. Abdulhameed, S. V. Surip, S. Sabar, Int. J. Environ. Anal. Chem. 100, 1-20 (2020). DOI: 10.1080/03067319.2020.1807966.
[45] F. Bouaziz, M. Koubaa, F. Kallel, R.E. Ghorbel, S.E. Chaabouni, Int. J. Biol. Macromolecule. 105, 56 (2017).
[46] M. Kiani, S. Bagheri, A. Khalaji, N. Karachi, Desal Water Treat. 226, 147 (2021).
[47] S. Banerjee, G. C. Sharma, P. K. Gautam, M. C. Chatto padhyaya, S. N. Upadhyay, Y. C. Sharma, J. Mol. Liquid. 213, 162 (2016).
[48] R. Istratie, M. Stoia, C. Pacurariu, C. Locovei, Arab. J. Chem. 12(8), 3704 (2019).

مجله شیمی فیزیک و شیمی نظری
دانشگاه آزاد اسلامی واحد علوم و تحقیقات
جلد ۱۸، شماره ۴، زمستان ۱۴۰۰
ISSN ۱۷۳۵-۲۱۲۶

مطالعات حذف رنگ متیل اورانژ با استفاده از نانوذرات اکسید آهن با پوشش گیاهی مارچوبه از محلول‌های آبی

علیرضا گرامی زادگان *

گروه مهندسی شیمی، واحد دشتستان، دانشگاه آزاد اسلامی، دشتستان، ایران

چکیده

کاربرد گیاه مارچوبه عامل دار شده با سنتز نانوذرات اکسید آهن برای حذف رنگ ها از محیط های آبی تایید شده است. تکنیک‌های FT-IR، BET، XRD و SEM برای بررسی، کاربرد گیاه مارچوبه عامل دار شده با نانوذرات اکسید آهن به عنوان جاذب برای حذف مناسب رنگ متیل اورانژ از محلول‌های آبی را نشان داد و مقادیر ۱۵/۰ میلی‌گرم در لیتر، ۰/۱ گرم را در مقاله نشان داد. ۷/۰، ۲۰/۰ دقیقه به ترتیب به عنوان مقادیر ایده آل برای غلظت رنگ متیل اورانژ، جرم جاذب، مقدار pH و زمان تماس در نظر گرفته شد. تعادل جذب و داده‌های جنبشی با مدل ایزوترم تک لایه لانگمویر (q: 0.9915) و سینتیک مرتبه دوم (R^2: 0.998) به ترتیب با حداکثر ظرفیت جذب (qmax: 167.7 میکروگرم بر گرم) برازش شدند. پارامترهای ترمودینامیکی (ΔG°: -11.42 kJ mol^{-1}، ΔH°: 33.3 kJ mol^{-1} K^{-1}، ΔS°: 145.8 kJ/mol^{-1} K^{-1})، همچنین نشان داد که جذب رنگ متیل اورانژ امکان‌پذیر، خود به خود و گرماگیر است. به طور کلی، با در نظر گرفتن راندمان عالی، احیای خوب و عملکرد قابل قبول در شرایط واقعی، نانوذرات اکسید آهن با پوشش گیاهی مارچوبه را می‌توان به عنوان یک جاذب امیدوارکننده برای حذف رنگ از محلول‌های آبی معرفی کرد.

کلید واژه‌ها: رنگ متیل اورانژ، ظرفیت جذب، ایزوترم، نانوذرات، انرژی جنبشی.

* مسئول مکاتبات: geramialireza42@gmail.com